Astron. Astrophys. 323, L37–L40 (1997)

ASTRONOMY AND ASTROPHYSICS

LETTER

Letter to the Editor

Soft X-ray emission and optical multicolors of faint QSOs in the Selected Area 57

T. Miyaji[12], **A.J. Connolly**[3], **A.S. Szalay**[3], **and E. Boldt**[4]

[1] Astrophysikalisches Institut, An der Sternwarte 16, D-14482 Potsdam, Germany (present address); (e-mail: tmiyaji@aip.de)
[2] Max-Planck-Institut für extraterrestrische Physik, D-85740 Garching b. München, Germany
[3] Department of Physics and Astronomy, Johns Hopkins University, Baltimore, MD 21218, USA (e-mail: ajc@pha.jhu.edu,szalay@pha.jhu.edu)
[4] Code 660, NASA Goddard Space Flight Center, MD 20771, USA (e-mail: boldt@lheavx.gsfc.nasa.gov)

Received 24 April 1997 / Accepted 13 May 1997

Abstract. We present the *ROSAT* HRI X-ray measurements of 19 spectroscopically confirmed optically-selected QSOs in the $12'$ radius region in the Selected Area 57. The optical-to-X-ray spectral index $\alpha_{\rm ox}$ ranges from 1.25 to 1.7, consistent with brighter QSOs. We have investigated the relationship between soft X-ray emission observed with the *ROSAT* HRI and optical colors (*UJFN*) of optically-selected QSOs in SA57. The optical to X-ray spectral index $\alpha_{\rm ox}$ is found to be correlated with the $U - J - F + N$ color, by a combined effect of $\alpha_{\rm ox}$ and U, N excess correlations. Possible explanations are the physical link between broad emission-lines/Balmer continuum, and the ionizing radiation source seen in X-ray and/or a geometrical effect.

Key words: Galaxies: active – X-rays: general

1. Introduction

This is the first paper reporting the ROSAT High Resolution Imager (HRI) observation of the Selected Area 57 (SA57). This field has been the subject of extensive extragalactic studies and is one of the fields with faint QSO searches with deep four-band multicolor photometry and spectroscopy data. Out of 77 objects which have a stellar image and colors unlike stars ($J \leq 22.5$) over 0.3 deg^2, 30 have been spectroscopically confirmed as QSOs (Koo, Kron, & Cudworth 1986, hereafter KKC; Koo & Kron 1988, hereafter KK88). A few more QSOs have been found by searching for variable objects and objects with no significant proper motion (e.g. Trevese et al. 1994, T94 hereafter). With these efforts, this field has a fairly complete sample of optically-selected QSOs without depending on the UV-excess criterion. Faint QSOs represent lower luminosity objects at a given redshift or higher redshift objects for a given luminosity than well-studied bright QSOs. Thus investigating these objects provides unique information on the properties and the evolution of the AGN population.

In this *letter*, we report the soft X-ray emission observed with *ROSAT* HRI from a sample of QSOs and correlation results of optical colors and the soft X-ray emission observed with *ROSAT* . A standard Friedmann universe with H_0 = 50[km s^{-1} Mpc^{-1}] and q_0 = 0 has been used in calculating luminosities.

2. The Optically-Selected QSO Sample

The QSOs have been drawn from the list of KK88 ($J < 22.5$) (see also KKC for color selection criteria). We have used the QSOs classified as 'B' (broad-line) by KK88 with a measured redshift located within $12'$ of the *ROSAT* pointing center. In addition, one QSO from T94 (NSER 8196) which has been missed in the KKC color criteria has also been included. This gives a sample of 19 optically-selected QSOs. The QSOs used in the analysis are listed in Table 1, sorted by redshift. Table 1 shows the QSO number assigned by KKC, the serial number of the SA57 photometry catalog (NSER), coordinates, the J magnitude, and quantities from X-ray and optical observations described later. Optical magnitudes in three other bands (U, F, and N see KKC), have also been used in the analysis. The response curves of the four photometric bands and discussion of random errors associated with the magnitudes of faint objects can be found in Koo (1985;1986).

3. The ROSAT HRI observation

The SA57 field was observed with the *ROSAT* HRI (High Resolution Imager; David et al. 1994) with 106 ks and 67 ks of

Send offprint requests to: T. Miyaji, AIP address

Table 1. QSOs in SA57 used in the Analysis (off-axis angle $< 12'$)

KKC	NSER	α (J2000)	δ	z[a]	J [mag]	$(f_{x14}^{(0.5-2keV)} \pm \sigma)[10^{-14}$erg s^{-1}cm$^{-2}]$ (1st obs.)	(2nd obs.)	(sum)[b]	log $L_x^{(0.5-2keV)}$ [erg s^{-1}]	α_{ox}
...	8169	13:08:01.5	29:20:08	0.74	21.92	<0.5	<0.7	<0.4	<43.28	>1.43
46	13966	13:08:44.0	29:28:39	0.95	21.30	0.5±0.1	0.7±0.2	0.6±0.1	43.70	1.47
36	11450	13:08:30.3	29:25:01	0.96	22.31	<0.3	<0.4	<0.2	<43.26	>1.49
27	5643	13:08:15.7	29:16:12	0.98	21.17	1.5±0.3	1.6±0.3	1.6±0.2	44.16	1.34
64	5422	13:09:11.7	29:15:52	1.08	20.62	2.9±0.4	3.0±0.4	2.9±0.3	44.54	1.33
34	5141	13:08:27.1	29:15:25	1.09	20.60	3.0±0.3	1.1±0.3	(v)2.3±0.2	44.44	1.36
45	15248	13:08:42.0	29:30:43	1.14	22.29	<0.4	0.6±0.2	<0.4	<43.74	>1.40
43	7326	13:08:39.7	29:18:49	1.32	21.03	0.4±0.1	<0.4	0.3±0.1	43.80	1.63
23	4882	13:08:12.1	29:14:58	1.47	21.89	1.4±0.3	<0.9	(v)1.1±0.2	44.49	1.29
25	9980	13:08:13.1	29:22:43	1.54	20.24	0.8±0.2	0.5±0.2	0.7±0.1	44.34	1.57
28	7624	13:08:16.0	29:19:17	1.74	19.44	2.0±0.2	1.6±0.3	1.9±0.2	44.93	1.56
31	15180	13:08:24.2	29:30:36	1.80	21.13	0.9±0.2	1.0±0.2	1.0±0.2	44.71	1.41
37	7567	13:08:32.0	29:19:11	1.81	20.51	<0.2	<0.4	<0.2	<44.05	>1.70
50	3544	13:08:49.5	29:12:45	1.81	20.17	1.5±0.3	3.0±0.5	(v)2.1±0.3	45.03	1.40
58	13412	13:09:06.3	29:27:48	2.08	22.11	<0.4	<0.6	<0.3	<44.32	>1.44
30	9877	13:08:23.2	29:22:33	2.12	22.06	0.3±0.1	0.5±0.2	0.4±0.1	44.52	1.47
56	6442	13:09:04.7	29:17:29	2.12	22.29	0.6±0.2	1.2±0.3	(v)0.9±0.2	44.86	1.32
16	9934	13:08:06.0	29:22:38	2.53	22.27	<0.4	<0.5	<0.4	<44.69	>1.41
22	11610	13:08:11.8	29:25:12	3.02	19.56	0.6±0.1	<0.4	(v)0.5±0.1	45.12	1.70

[a] Redshifts are from KK88 except NSER 8169,13412 (T94), and 15180 (Borra et al. 1996). [b] (v):x-ray variable.

Table 2. Log of ROSAT HRI Observations on SA57

Pointing	$(\alpha, \delta)_{J2000} = (13^h08^m38.4^s, +29°22'48'')$	
Sequence	US900638H-1	US900638H-2
Start/End	6 June-3 July 1995	27 June-12 July 1996
Exposure	105.7 ks	66.7 ks

exposures separated by approximately one year. The log of observations is shown in Table 2.

In the whole HRI field, there are about 30 point or point-like X-ray sources and the nature of the X-ray sources are the topic of a future paper. It was straightforward to make the boresight correction with known QSOs. We have measured the X-ray counts from the *ROSAT* HRI data at the positions of the QSOs with the maximum-likelihood fitting procedure using the *EXSAS* package (Zimmermann et al. 1994) and treated objects with likelihood > 6 (roughly 3σ) as detected. We have limited our analysis to within $12'$ of the HRI pointing, beyond which the detection fraction of QSOs drops drastically because of the degraded PSF.

Since the current version of EXSAS (January 1996) assumes an off-axis angle dependent single gaussian profile for the PSF for the maximum-likelihood fitting, the fit usually underestimates the count rate. We have corrected for the effect by an extensive simulation using the David et al. (1994) two gaussian plus one exponential PSF. Upper-limit counts for non-detected sources, corresponding to the detection limit at a likelihood of 6, have been determined also from simulations.

An effective exposure map has been created for each observation using the *cast_exp_hri* software[1]. A photon spectral index of $\alpha_{ph} = 2.0$ (e.g. Hasinger 1993) with $N_H = 1.0 \times 10^{20}$cm^{-2} (the Galactic value for SA57;Dicky & Lockman 1990) has been assumed to convert the corrected count-rate to the unabsorbed flux in $0.5 - 2$ keV. The conversion factor between the corrected HRI count rate to *unabsorbed* 0.5 – 2 keV flux is then 1.9×10^{-11}erg s^{-1}cm^{-2} (cts s^{-1})$^{-1}$. Table 1 shows the QSO sample and X-ray fluxes for each of two observations and the summed data. The X-ray luminosities L_x have been calculated from the summed data and the same spectral assumption has been used for the K-correction. Comparing the fluxes in two separate observations, five QSOs show a significant variability by a factor of 2 – 3.

4. Soft X-ray Emission and Optical Colors of QSOs

4.1. Luminosities and α_{ox}

We have calculated the pseudo optical-to-X-ray spectral index $\alpha_{ox} = 0.38[\log L_\nu(2500Å) - L_\nu(2\,\mathrm{keV})]$, where $L_\nu(2500Å)$ and $L_\nu(2\mathrm{keV})$ are monochromatic luminosities of the QSO continuum emission at 2500Åand 2 keV (from the summed data) at the source rest frame respectively. For the 2500Å luminosity calculation, we have applied corrections for the existence of emission-lines considering the same set of lines and equivalent widths as Marshall et al. (1983). The magnitude-to-

[1] The *cast_exp_hri* software, created by S. L. Snowden, has been obtained from the High Energy Astrophysics Archival Research Center, operated by NASA Goddard Space Flight Center.

flux conversion has been made based on Table 9 of Fukugita, Shimasaku, & Ichikawa (1995) and calculated the monochromatic flux at $2500(1+z)$ Å from the fluxes at the closest two of the emission-line corrected *JFN* fluxes by a logarithmic inter- or extra-polation. The spectral dependence of the conversions, slight offsets of the α Lyr magnitudes from zero, and the small Galactic extinction in SA57 ($E[B-V] = 0.002$) are much smaller than the possible systematic errors of the data reduction and thus have been neglected. The $\alpha_{\rm ox}$ value (Table 1) range from 1.25 to 1.7, consistent with the values for the brighter samples (e.g. Green et al. 1995).

4.2. Optical Multicolor – $\alpha_{\rm ox}$ Correlations

We have explored the correlation properties between $\alpha_{\rm ox}$ and the optical color of the QSOs. Although each band corresponds to a different source-rest frame wavelength for each QSO, we searched for a general trend in hope that this could lead to a qualitative discussion which would lead to a further investigation. Some color-$\alpha_{\rm ox}$ scatter diagrams are shown in Fig. 1 (a)-(d). The $U-J-F+N$ color is the measure of the second derivative of the overall optical spectrum (bowl or hump shaped).

Fig. 1 shows that $\alpha_{\rm ox}$ seems correlated with $U-J-F+N$ color and possibly with $U-J$ and $J-N$. We have assessed the significance of the correlations using the survival analysis package ASURV (La Vally, Isobe, Feigelson 1992), since 6 of the 19 QSOs have only upper-limits to the X-ray flux. If $N > 21$, we treated the listed N magnitude minus the error by Koo (1985) as its lower-limit. Thus for the colors including N, we have doubly censored data. The generalized Kendall's τ can be used to assess the significance in such cases. The results are listed in Table 3, showing the probability that correlation does *not* exist between the colors and $\alpha_{\rm ox}$. Cox's proportional hazard model has also been used when applicable and shown following the slash. The results did not change significantly when the nominal value of N was used instead of the lower-limit or the objects with $N > 21$ was neglected. The results didn't change significantly either when we used only the first or second X-ray observation.

Table 3 shows that the correlation between $\alpha_{\rm ox}$ and $U-J-F+N$ is significant at a 99.6% level and contributed by both infrared (in the observer's frame) and ultraviolet excesses. Instead of $\alpha_{\rm ox}$, we have also used the ratios of the X-ray to U and N band fluxes ($J+2.5\log f_{\rm x}$ and $N+2.5\log f_{\rm x}$, denoted by *U-X* and *J-X* respectively). The correlations are not significant or much weaker in those cases. Fig. 1 also shows that the correlation is not simply the sequence of the spectral shift of z. We have plotted the spectral energy distributions (SEDs) of selected QSOs which occupy two ends of the scatter in Fig. 1(d), in the object's rest frame (Fig. 2). Fig. 2 shows that the SEDs of the QSOs indeed range from hump to bowl.

5. Discussion

The optical color $\alpha_{\rm ox}$ correlation could only be established since the QSO selection does not depend on the UV-excess technique

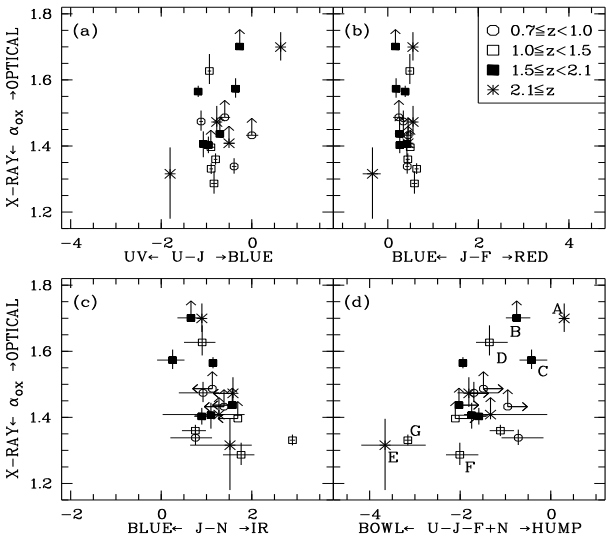

Fig. 1. The correlations between optical colors (uncorrected for emission lines) and $\alpha_{\rm ox}$ are shown. Different symbols correspond to different redshifts as indicated. The SEDs of labeled objects in panel (d) are shown in Fig 2

Table 3. Probability that correlation is *not* present (%)

	$U-J$	$J-F$	$J-N$	$U-J-F+N$
$\alpha_{\rm ox}$	8./3.	48./87.	1.	0.4
U-X	55./33.	10./39.	24.	10.
N-X	66.	95.	95.	52.

and this is one of the unique features of the QSO sample in SA57. Possible bias due to variability effects would not make the apparent correlation, since the gap of more than 15 years between optical and X-ray observations would tend to randomize $\alpha_{\rm ox}$ and thus weaken the possible bias. This is also shown by the fact that using the X-ray data from the first or second sequence (Table 2) alone instead of summed data did not change the results significantly. Also the span of $\alpha_{\rm ox}$ distribution, corresponding to a factor of $\sim$10, is larger than the QSO variability in X-ray (this work) and optical (T94), which are about a factor of two or three at most. From the correlations shown above, the U (1000-1500 Å at QSOs) and N (2500-4000 Å at QSOs) emission seems to be linked with the X-ray emission (2-3 keV at QSOs), while the emission around 1500-2500Å consists of a separate component. Many factors can affect the overall SED in this range, making a complex variety of spectral behavior: (1) the non-thermal power-law component (2) the small (3000Å) bump, probably the Balmer continuum (3) the big blue bump (probably thermal emission from accretion disk) (e.g. Malkan & Sargent 1982) (4) emission lines (5) the QSO intrinsic and intergalactic absorptions.

Probably the X-rays from the QSOs mainly come from the central non-thermal component, except for a part of those with $z \lesssim 1$, which may be contaminated by the 'soft excess' component seen in some nearby Seyfert 1's at $E \lesssim 1$keV, because of

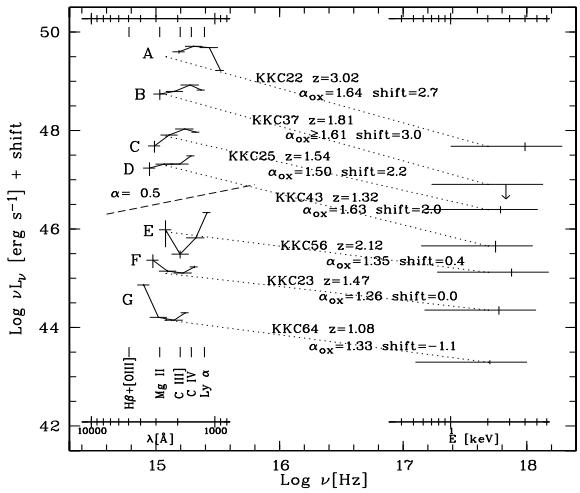

Fig. 2. The SEDs of selected QSOs, labeled by A-E to indicate the correspondences with objects in Fig.1(d), are plotted in the object's rest frame. Emission-line corrections haven't been made for this plot. The horizontal error bars roughly show the widths of photometric bands or the HRI response. Vertical 1σ error bars include only random photometry errors. The 2500Åand 2 keV luminosities, from which α_{ox} has been calculated, (see text) are connected by a dotted line. For reference, an α = 0.5 power-law spectrum, average for the optical continuum of bright QSOs in Richstone & Schmidt (1980) (dashed line) and positions of major emission lines are shown

the HRI's sensitivity extending below E = 0.5 keV. The effect could lead to an overestimate of the 2 keV luminosity by a factor of two for a $z \lesssim 1$ QSO with a strongest soft-excess. This is not likely to be the main source of correlation, where the objects in the whole redshift range are involved and the flux ratio spans by a factor of 10. The optical continuum, in particular around the J band, the big blue bump is probably dominant for most of the sample QSOs.

Among the bowly objects shown in Fig.2, U-band in KKC 22 (z=3.02) corresponds to the source rest frame beyond the Lyman-limit and the strong drop can be explained by the intrinsic and/or intergalactic Lyman absorption. The J-band bump of KKC 37 and KKC 25 may be contributed by the broad CIV emission line.

The U and N excesses in the three bowly objects (E-G in Fig. 2) can be significantly contributed by strong broad emission lines (Lyα and CIV) and the small bump (the Balmer continuum). In fact, Green (1996) found a strong anti-correlation between the Lyα equivalent width and α_{ox} for his large sample of low-redshift QSOs, but not for the broad CIV line. If the main source of the color - α_{ox} correlation comes from Lyα and Balmer continuum, this suggests that the main source of hydrogen ionization comes from the non-thermal source rather than the thermal emission from the accretion disk. A geometrical effect, where the non-thermal and line emissions are isotropic while the observed flux of the thermal emission depends on the viewing angle (stronger when it is seen face-on), can also contribute to the observed correlation. Good spectrophotometric measurements would be needed for further quantitative discussions. Note that the very strong J and U excess in KKC 56 is not likely to be solely due to the emission lines, even though an unusually strong CIV line is present in our unpublished spectrum. This particular object has unusual colors with strong X-ray emission and thus is an interesting object for further followup observations.

Acknowledgements. TM appreciates the hospitality of/support from NASA/GSFC, USRA, and the Johns Hopkins Univ. during his visits. The authors thank Julian Krolik and David Koo for useful comments.

References

Borra E.F., Levesque S., Beauchemin M. et al. 1996, AJ, 111, 1456
David L.P., Harnden F.R. Jr., Kearns K.E., Zombeck M.V. 1995, The *ROSAT* High Resolution Imager (HRI)
Dicky J.M., Lockman F.J. 1990, ARA&A 28, 215
Fukugita M., Shimasaku K., Ichikawa T. 1995, PASP 107, 945
Green P.J. 1996, ApJ 467, 61
Green P.J., Schartel, N., Anderson, S.F. et al. 1995, ApJ 450, 51
Hasinger G., Burg R., Giacconi R., et al. 1993, A&A 275, 1
Koo D.C. 1985, AJ 90, 419
Koo D.C. 1986, ApJ 311, 651
Koo D.C., Kron R.G., Cudworth K.M. 1986, PASP 98, 285 (KKC)
Koo D.C., Kron R.G. 1988, ApJ 325, 92 (KK88)
La Valley M., Isobe T. & Feigelson E.D. 1992 in Astronomical Data Analysis Software and Systems, ed, D. Worrall et al. (San Francisco: ASP), 245
Malkan M.A., Sargent W.L.W 1982, ApJ 254, 22
Marshall H.L., Tanabaum H., Zamorani A. et al. 1983 ApJ 269, 42
Richstone D.O., Schmidt M. 1980, ApJ, 235, 361
Trevese D., Kron R.G., Majewski S.R., Bershady M.A., Koo D. 1994, ApJ 433, 494 (T94)
Zimmermann H.U., Becker W., Belloni T. et al. 1994, EXSAS User's Guide, MPE Report 257, (Garching:MPE)

This article was processed by the author using Springer-Verlag LaTeX A&A style file *L-AA* version 3.